

## **Geophysical Research Letters**

#### RESEARCH LETTER

10.1029/2018GL079185

#### **Kev Points:**

- Steep-dipping ramp causes fast shear stress accumulation and hence early coseismic failure in both shallow and deep segments
- Stronger frictional strength allows more shear stress accumulation and hence later coseismic failure
- The hypothesis of shallow strain reservoir may be related to strong frictional strength and shallow-dipping angle of the fault

#### Correspondence to:

S. Li, shaoyang-li@uiowa.edu

#### Citation:

Li, S., Barnhart, W. D., & Moreno, M. (2018). Geometrical and frictional effects on incomplete rupture and shallow slip deficit in ramp-flat structures. *Geophysical Research Letters*, 45, 8949–8957. https://doi.org/10.1029/2018GL079185

Received 12 JUN 2018 Accepted 19 AUG 2018 Accepted article online 27 AUG 2018 Published online 6 SEP 2018

# Geometrical and Frictional Effects on Incomplete Rupture and Shallow Slip Deficit in Ramp-Flat Structures

Shaoyang Li<sup>1</sup> , William D. Barnhart<sup>1</sup> , and Marcos Moreno<sup>2,3</sup>

<sup>1</sup>Department of Earth and Environmental Sciences, University of Iowa, Iowa City, IA, USA, <sup>2</sup>GFZ Helmholtz Centre Potsdam, German Research Centre for Geosciences, Telegrafenberg, Potsdam, Germany, <sup>3</sup>Departamento de Geofísica, Facultad de Ciencias Físicas y Matemáticas, Universidad de Concepción, Concepción, Chile

**Abstract** Several recent moderate-magnitude ( $M_w > 7$ ) earthquakes, such as the 2015 Gorkha, Nepal, ruptured only the deep (>15 km depth) portions of megathrust faults, leaving the updip sections unbroken. Here we investigate the effects of geometrical and frictional variations at depth on the stress accumulation and release in ramp-flat structures using 2-D finite element models. Our results show that ramp-flat structures allow for faster but lower shear stress accumulation with increasing dip of the deep ramp section while increasing frictional strength of the faults allows more stress accumulation. These factors lead to earlier yet smaller failures of the ramp followed by larger and less frequent failures affecting the shallow section. Our models thus suggest that the dynamics of strain reservoirs are related to both the frictional strength and dips of ramp-flat megathrust structures, and the failure time of the shallow fault section is affected by the stress regime at the deep fault segment.

**Plain Language Summary** Many recent earthquakes only rupture in deep (>15 km depth) with the shallow portion of the fault unbroken in a longer time, including the case of the 2015  $M_{\rm w}$  7.8 Gorkha Nepal earthquake in the central Himalayan arc. A few historical earthquakes seem also rupture only the deep portion, with much stress unreleased in the shallow portion as a stress "reservoir." It is unclear how these phenomena are related to fault friction and geometry properties. We used numerical models to study the influences of these properties on stress accumulation during the interseismic period and on the time of final coseismic break. We found that comparing to shallow-dipping fault, steep-dipping fault can cause faster stress accumulation but is capable of sustaining lower stress in total, so it tends to break in a shorter time. On other hand, stronger frictional strength allows more stress accumulation in a longer time before the earthquake. In this way, the shallow portion of a fault with low dip angle and high frictional strength can be very stable in a long time and even absorbs stresses from earthquakes of the deep portion. So the shallow portion of this kind of fault is capable of hosting a very large earthquake.

#### 1. Introduction

Recent detailed earthquake studies highlight that there is a population of moderate- to large-magnitude earthquakes ( $M_w > 7$ ), termed zone-C events (Lay et al., 2012), that rupture the deeper portions of plate boundary thrust faults in regions where larger ( $M_W$  8-9+) earthquakes are known or suspected to have occurred (e.g., Barnhart et al., 2018; Beck et al., 1998; Bilham & England, 2001; Delouis et al., 2009; Elliott et al., 2016; Hayes et al., 2014; linuma et al, 2011; Konca et al., 2008; McNamara et al., 2017; Melgar et al., 2017; Moreno et al., 2018; Okada et al., 2005; Schurr et al., 2012; Simons et al, 2011). For example, the 2016  $M_{\rm w}$  7.6 Melinka, Chile earthquake partially ruptured a downdip portion of the 1960 M 9.5 Valdivia earthquake source region (Melgar et al., 2017; Moreno et al., 2018) and the 2015 M<sub>w</sub> 7.8 Gorkha, Nepal earthquake and its largest aftershock partially ruptured the Main Himalayan Thrust (MHT; e.g., Avouac et al., 2015; Elliott et al., 2016; Hayes et al., 2015; Mencin et al., 2016). These moderate-magnitude events reflect incomplete ruptures of fault segments that later can rupture as great earthquakes, and the greater frequency of these moderatemagnitude earthquakes lead to a heterogeneous strain distribution that may influence the timing and spatial distribution of subsequent earthquakes through the generation of an updip strain reservoir (e.g., Mencin et al., 2016). Consequently, understanding why these deeper, more frequent moderate-magnitude earthquakes occur and why they fail to rupture the entire updip portion of the thrust can inform regional seismic hazard and the properties of faults that control earthquake segmentation.

©2018. American Geophysical Union. All Rights Reserved.



The mechanisms underlying these incomplete ruptures and the development of strain reservoirs remain enigmatic. Broadly, two end-member properties have been proposed to explain this mechanical segmentation: frictional heterogeneities and geometric heterogeneities at depth. Both of these possibilites are exemplified by the 2015 Gorkha, Nepal earthquake. The Gorkha earthquake ruptured the downdip portion of the MHT in a region encompassing along-dip geometric changes, or "ramp-flat" structures (Zhao et al., 1993; Schulte-Pelkum et al., 2005; Hubbard et al., 2016), which are frequently observed in continental collision zones or subduction zones, for another instance, in the Zagros Mountains (e.g., Barnhart et al., 2018). Geodetic and seismic investigations of the Gorkha earthquake revealed that coseismic slip concentrated near the geometric transition of the flat to the ramp segment at ~15 km depth, and negligible, seismic or aseismic, slip propagated to the shallow depth (<10 km; Elliott et al., 2016; Mencin et al., 2016; Qiu et al., 2016; Zhang et al., 2017). The lack of fault slip in the updip flat portion of the MHT indicates that this portion of the megathrust absorbed considerable elastic strain that has not yet been released. Previous earthquakes in this region exhibited similar behavior, leading to the hypothesis that shallow portion of the megathrust may act as strain reservoir, with elastic energy tranferred and stored from deep, more frequent but smaller ruptures until a great earthquake eventually sweeps through these shallow regions (Bilham et al., 2017). These observations suggest that downdip seismogenic segmentation of the MHT is geometrically controlled (e.g., Qiu et al., 2016; Lindsey et al., 2018), as has been suggested in other regions (e.g., Bletery et al., 2016; Duan, 2012; Yang et al., 2013). However, slip distributions of the Gorkha earthquake mimic incomplete ruptures in other regions where incomplete rupture seem to be depth-controlled, which is consitent with the notion that a plate boundary thrust is zoned according to frictional strength variations (e.g., Konca et al., 2008; Perfettini et al., 2010; Lay et al., 2012; Moreno et al., 2018). Previous numerical studies showed that depth-varying friction may influence the earthquake size and timing (e.g., Gao & Wang, 2017; Moreno et al., 2018; Murphy et al., 2018).

In this study, we explore the interplay between friction and geometric heterogeneities of thrust faults, and how they contribute to cycles of incomplete and full-fault ruptures along large thrust faults. We establish a suite of 2-D mechanical models to simulate the earthquake cycle in the presence of both frictional and geometric variations as a means to quantitatively describe the relative impacts of these properties on interseismic stress accumulation, earthquake frequency-magnitude relationships, and the relative time to complete fault failure. We use observations of the Gorkha earthquake and the paleoseismic history of the central Himalayan Arc to calibrate our models in locales where it is inferred that the entire thrust interface is capable of coseismic slip.

#### 2. Methods

To investigate the competing contributions of friction and variable fault geometry on the earthquake cycle of a thrust fault, we developed a suite of 2-D mechanical models with the open-source finite element code PyLith (Aagaard et al., 2013). To simulate the steady interseismic loading, we implement the previously reported kinematic elastic plate model of Kanda and Simons (2010; Figure 1a). In this model, the entire base of the downgoing plate (assigned a thickness of 40 km) and the top of the downgoing plate below the seismogenic zone are allowed to creep freely at a convergence rate (i.e., 20 mm/year (Lavé & Avouac, 2000; Loveless & Meade, 2011)) and the seismogenic zone is defined as the contact interface between the downgoing and overriding plates. The seismogenic zone extends from the surface to 25-km depth based on source models the 2015 Gorkha earthquake (e.g., Avouac et al., 2015; Elliott et al., 2016; Feng et al., 2017; Galetzka et al., 2015; Hayes et al., 2015; Lindsey et al., 2015; McNamara et al., 2017; Yue et al., 2017) and is assigned velocity-weakening friction behavior (Scholz, 1998; described later in this section). In doing so, continuous motion of the downgoing plate and frictional locking of the seismogenic zone mechanically drive the interseismic stress accumulation in the system until there is frictional instability (coseismic slip) on the fault interface. In each simulation during the period that the fault is fully locked, we track the shear stress accumulation rate ( $\kappa$ ) along the fault and the velocity field (e.g., Figures 1b and 1c), which are dependent on the setups of material properties, boundary conditions, and fault geometry.

Following the generalized geometry of the MHT in the central Himalayan Arc, the shallowest (≤15 km) portion of the seismogenic zone is characterized as the shallowly dipping "flat," while the deeper (>15 km) portion is characterized as the more steeply dipping "ramp". We then iteratively vary the dip angles of the ramp segment from 7 to 40°. We additionally generate simulations with no depth-dependent dip variations. For

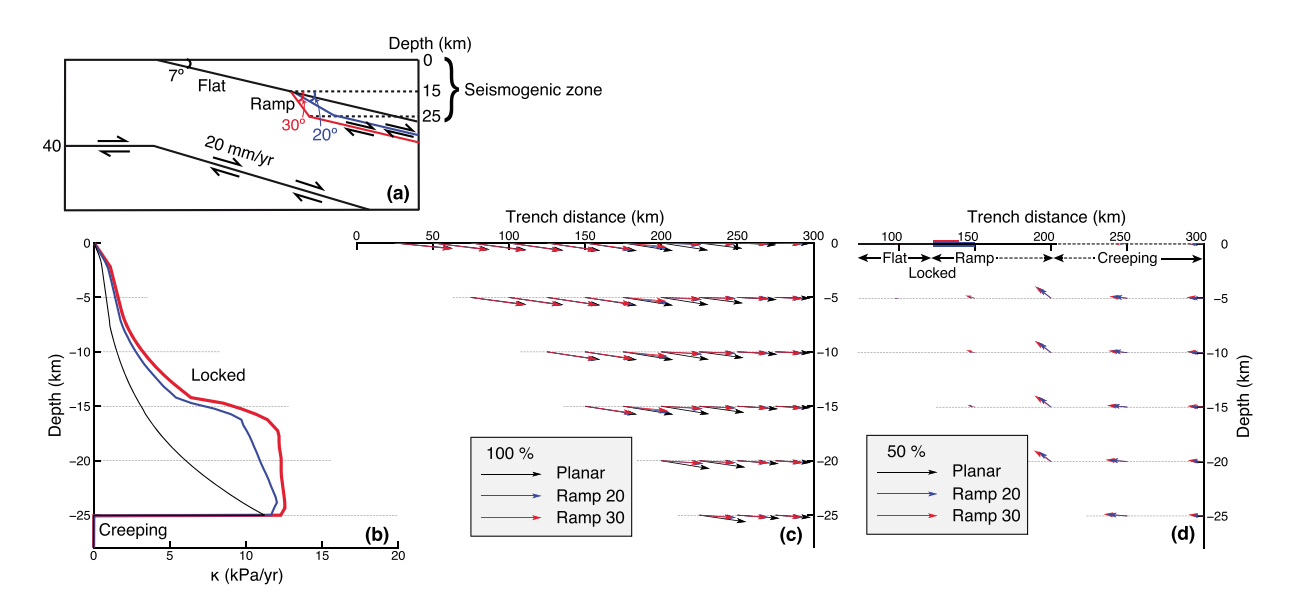


**Figure 1.** Geometrical (fault dipping) effects on shear stress accumulation  $\kappa$  along the fault interface and deformation pattern in the hanging wall during the interseismic period. (a) Elastic plate model (Kanda & Simons, 2010) setup and test geometries (not to scale): The planar fault and two ramp-flat faults. Blue and red lines show the ramp segments of the ramp-flat faults. (b) Shear stress accumulation rates of different fault geometries under the same tectonic loading. (c) Velocities normalized by the plate convergence rate (in percentage) in the hanging wall with different fault geometries under the same tectonic loading. (d) Differences of normalized velocities of the planar fault model and ramp-flat fault models. The scales of the velocities are enlarged 2 times comparing Figure 1c. The three fault segments are projected onto the horizontal axis.

simplicity, we assign uniform elastic material properties to both the upper and lower plates, with a shear modulus of 30 GPa and a Poisson's ration of 0.25. In this setup, any variations between model runs should depend solely on the imposed fault dips and frictional coefficients. The variation in imposed fault dips inherently affects the area of the seismogenic zone (i.e., the planar fault has a larger area of seismogenic zone than ramp-flat fault; Figure 1a). In our simulations, we do not allow for the occurrence of rupture of splay faults; thus, all slip is accommodated by a single plate boundary structure.

In order to simulate fault failure, we impose the Coulomb failure criterion on the seismogenic portion of the fault (Jaeger & Cook, 1979):

$$\Gamma = \mu' \sigma + c \tag{1}$$

where  $\Gamma$  is the absolute shear strength resolved onto the fault,  $\mu'$  is the effective friction coefficient,  $\sigma$  is the fault normal stress, and c is the fault cohesion. Here  $\mu'$  includes the typical frictional sliding coefficient ( $\mu_0$ ) and the effects of pore fluid pressure ( $\lambda$ ), that is,  $\mu' = \mu_0(1 - \lambda)$ . The occurrence of earthquakes has long been hypothesized to result from a stick-slip frictional instability (Ruina, 1983). Such instability is described as a sudden drop of  $\mu'$  ( $\Delta\mu'$ ) from a preseismic static value to a coseismic dynamic value, causing the weakening of the fault strength ( $\Delta\Gamma$ , strength drop):

$$\Delta\Gamma = \left(\mu'_{\text{static}}\sigma + c\right) - \left(\mu'_{\text{dynamic}}\sigma + c\right) = \Delta\mu'\sigma \tag{2}$$

We assume that the modeled system is in lithostatic equilibrium and the normal stress along the fault equals the force due to the gravity of the overlying rock column, which is invariant before and after the earthquake.  $\Delta\Gamma$  can thus be further written as

$$\Delta\Gamma = \Delta\mu' \ \rho gh\cos \theta \tag{3}$$

where  $\rho$  is the density, g is the gravitational acceleration, h is the fault depth, and  $\theta$  is the fault dip. For simplicity,  $\rho$  is assumed to be 2,700 kg/m³, and g is 9.80665 m/s². Fault instability occurs when the accumulated shear stresses ( $\Delta \tau$ ) exceed  $\Delta \Gamma$ ; for example,  $\Delta \Gamma$  defines the maximum shear stress ( $\Delta \tau_{max}$ ) that the seismogenic zone is capable of accumulating during the interseismic period ( $\Delta \tau_{max} = \Delta \Gamma = \Delta \mu' \rho ghcos\theta$ ). For a typical great earthquake,  $\Delta \tau_{max}$  is on the scale of 1 to 10 MPa (Allmann & Shearer, 2009). This equates to an effective



friction coefficient drop ( $\Delta \mu'$ ) of 0.01 at 20-km depth (~5 MPa). Since normal stress is proportional to fault depth, higher  $\Delta \mu'$  is indicative of larger earthquake size.

In addition to the geometry of the ramp-flat segment, we iteratively vary  $\Delta\mu'$  (0–0.02) on both the shallow and deep segments. We note that the order of magnitude of  $\Delta\mu'$  is consistent with the values inferred from heat flow measurements (e.g., Gao & Wang, 2014) and geodynamic and analytical modeling results (e.g., Gerya et al., 2015; Kaneko et al., 2010; Wang & Hu, 2006), but lower than the values measured in laboratory sliding experiments (e.g., Di Toro et al., 2004; Goldsby & Tullis, 2011). We simulate a total time of 3,000 years of steady loading for each model iteration, and the time when the fault starts to slip is retrieved as the failure time. We do not include dynamic rupture and nucleation physics in our simulations (e.g., Michel et al., 2017). Rather, we focus on the time length needed to overcome  $\Delta\mu'$  and initiate stick-slip events under the steady tectonic loading. Therefore, our model informs the magnitudes of stress and time that the seismogenic zone can support before rupturing in moderate ( $M_w > 7$ ) to large ( $M_w > 8$ ) earthquakes.

#### 3. Results

We first investigate the impacts of fault dip variations on the rate of shear stress accumulation ( $\kappa$ ) along the fault interface and the displacement velocities in the hanging wall (Figure 1). For a planar fault (i.e., no depth variation in fault dip),  $\kappa$  increases nonlinearly with depth (Figure 1b). This indicates that there is a first-order control on  $\kappa$  introduced by the thickness of the hanging wall. In the simulation with varying dip between the ramp and flat segments,  $\kappa$  of the ramp segment increases at a higher rate than in scenarios where there is no variation in fault dip (Figure 1b). This accelerated stress accumulation is particularly pronounced at the transition point between the flat and ramp segments. Interestingly, with the presence of ramp segment, the rate of shear stress accumulation within the updip flat segment also increases compared to the shear stress accumulation rates at the same depth in the planar fault simulations. For instance, the ramp-flat fault with a 20° dipping ramp segment and a 7° dipping flat segment accumulates shear stresses at rates of ~7 and ~2 kPa/year faster than the planar fault at depth of 20 and 10 km, respectively (Figure 1b). With higher dip angles of the ramp,  $\kappa$  accumulates at increasingly higher rates (Figure 1b). Under the same tectonic loading, faults with a ramp-flat geometry induce smaller horizontal and vertical displacements in the hanging wall in comparison to the planar fault (Figure 1c). The normalized velocity differences between the ramp-flat model and the planar model (Figure 1d) indicate that the extending and uplifting deficits are built up immediately above the ramp segment in the hanging wall of flat-ramp model in comparison to the planar fault model.

We then explore the geometrical and frictional controls on  $\Delta \tau_{max}$  for a realistic earthquake (approximately a few megapascal stress drop) along the fault interface. In simulation where we impose a constant fault dip,  $\Delta \tau_{max}$  is linearly dependent on  $\Delta \mu'$  and depth to the fault plane (i.e., Byerlee's law, Byerlee, 1978; Figure 2). With increased dip angles, normal stress resulting from the vertical load of rocks decreases, and  $\Delta \tau_{max}$  additionally decreases as a result. We term this effect the "geometric stress deficit" in this study. For instance, for  $\Delta \mu' = 0.01$ , a 30° dipping fault accumulates 0.7 MPa of shear stress less than the 7° dipping fault at a depth of 20 km (Figure 2a). We also find the distribution of  $\Delta \tau_{max}$  depends on  $\Delta \mu'$ . Higher  $\Delta \mu'$  results in larger  $\Delta \tau_{max}$  that is proportional to the normal stress. We term this effect the "frictional stress reservoir" in this study. For instance, for a fault dipping of 7°, faults with  $\Delta \mu' = 0.02$  can accumulate 2.6 MPa more shear stress than the fault with  $\Delta \mu' = 0.01$  at depth of 10 km (Figure 2b).

The combination of  $\kappa$  and  $\Delta\tau_{max}$  determines the Coulomb failure time of the fault. To better understand the geometrical and frictional effects on the failure time, we investigate two scenarios: (1) a ramp-flat structure wherein we impose a uniform  $\Delta\mu'$  along the entire seismogenic zone and vary the dip of the deeper ramp segment (Figure 3a) and (2) a planar fault (no depth-dependent dip variations) wherein we impose depth-dependent variations in  $\Delta\mu'$  along the shallow and deep segments (Figure 4a). For case 1, we find that the failure time of the deep ramp segment decreases (i.e., shorter earthquake recurrence intervals) as dip increases (Figure 3b). This means that steeper dipping faults are prone to slip at earlier time than shallower dipping faults under the same loading condition and with the same fault friction properties. The variations in failure time induced by variations in fault dip are also influenced by  $\Delta\mu'$  (Figure 3b). With increasing  $\Delta\mu'$ , the effect of dip on failure time becomes more pronounced. For instance, when dip is increased from 7° to 40°, the reduced time to failure in the ramp segment under our loading conditions is ~1,000 years for  $\Delta\mu' = 0.004$ , but only ~200 years for  $\Delta\mu' = 0.001$ . Because steeper dip angles induce increased  $\kappa$ 

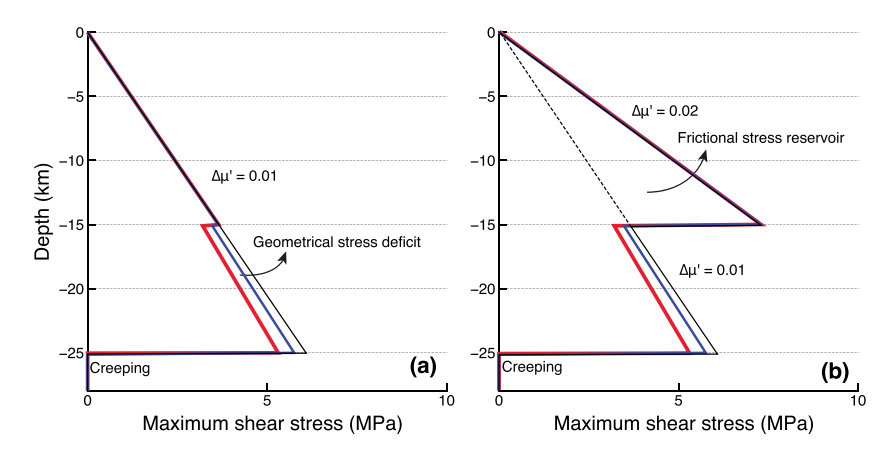


**Figure 2.** Geometrical and frictional effects on  $\Delta \tau_{\text{max}}$  along the fault interface. Black, blue, and red curves are, respectively, from planar and ramp-flat faults with 20° and 30° dipping angles as shown in Figure 1a. (a) Assumed uniform  $\Delta \mu'$ . (b) Assumed segmented  $\Delta \mu'$ .

(Figure 1b), the shallow, shallowly dipping "flat" segment always slips later than the deep, steeply dipping "ramp" segment. The time lag between these fault and ramp failures increases with the increasing dip of the ramp segment (Figure 3c). More interestingly, even for the case of planar fault, the shallow segment breaks later than the deep segment (positive values at the vertical dashed line in Figure 3c), because  $\kappa$  increases exponentially with depth if there is no geometrical variation along the fault (black curve in Figure 1b). Again, the increased time lag between the failure of the upper and lower segments also depends on  $\Delta\mu'$ . With larger  $\Delta\mu'$ , the effect of  $\theta$  on the time lag becomes more significant (i.e., the slope of the curve increases with  $\Delta\mu'$  in Figure 3c). For instance, when  $\theta$  is increased from 7° to 40°, the failure time lag of flat segment increases ~500 years for  $\Delta\mu' = 0.004$  but ~50 years for  $\Delta\mu' = 0.001$ .

For case 2, we find that the failure time of shallow/deep segment is predominantly controlled by  $\Delta\mu_1^{'}/\Delta\mu_2^{'}$  (Figures 4b and 4c), meaning that a longer time is required for one segment to overcome a larger frictional weakening of this segment. Furthermore, we find that the failure time of one segment is also influenced by

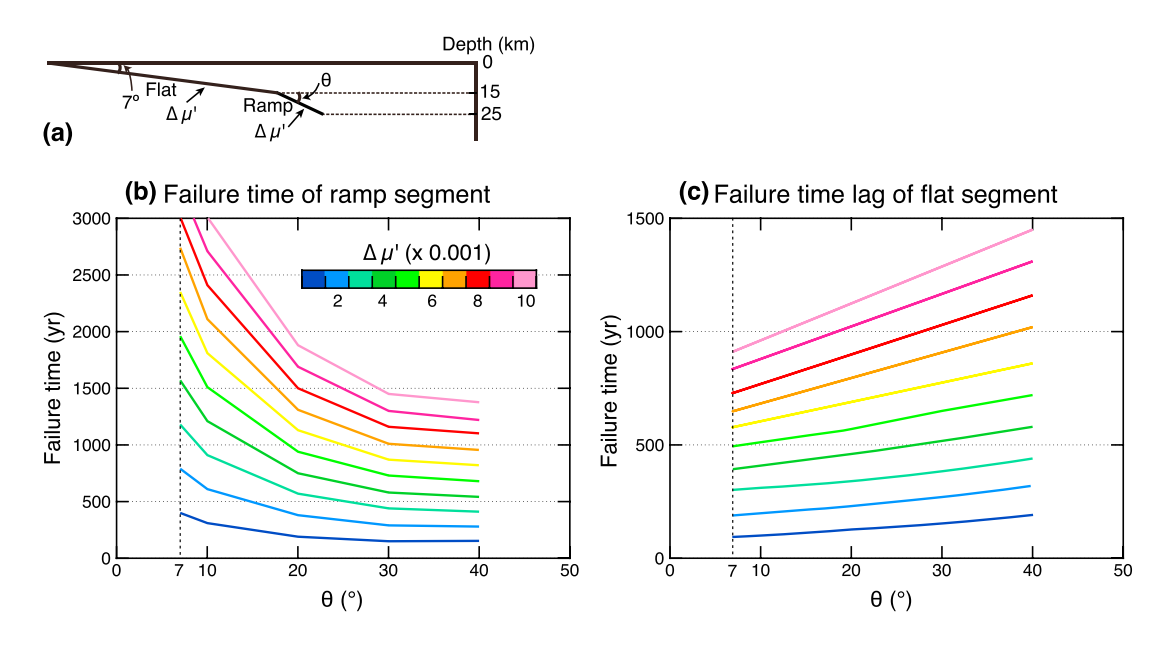


**Figure 3.** Geometrical effects on inferred rupture time along frictionally homogeneous fault. (a) Sketch illustrates the tested variables. (b) Failure time of the ramp segment. Dip angle, quick rupture of dipper segment, but also shallow segment. (c) The failure time lag between the flat and ramp segments (i.e., the failure time of flat segment minus the failure time of the ramp segment). Vertical dashed line shows the results of planar fault model.

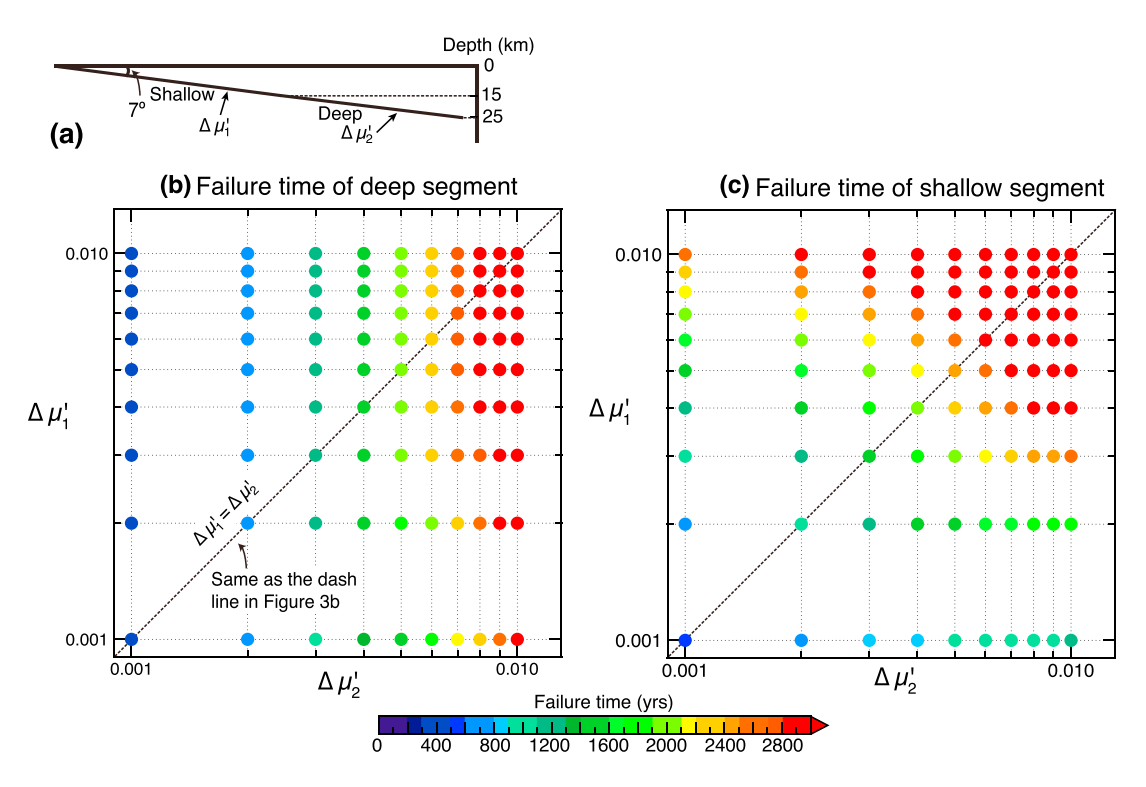


Figure 4. Frictional effects on inferred rupture time along planar fault. (a) Sketch illustrates the tested variables. (b and c) The failure time of the shallow and deep segments, respectively.

the strength of the other segment. The effect of  $\Delta\mu'$  of the shallow segment to the rupture time of the deep segment is weaker than the influence of  $\Delta\mu'$  of the deep segment on the failure time of the shallow segment. The failure time of the deep segment is far more sensitive to its own  $\Delta\mu'$  than to the changes in  $\Delta\mu'$  on the shallow segment. For instance, given  $\Delta\mu_2' = 0.006$ , the failure time of deep segment increases ~500 years when  $\Delta\mu_1'$  increases from 0.001 to 0.01 (Figure 4b), while given  $\Delta\mu_1' = 0.006$ , the failure time of shallow segment increases >1,000 years when  $\Delta\mu_2'$  increases from 0.001 to 0.01 (Figure 4c). We iterate here that when  $\Delta\mu_1' = \Delta\mu_2'$ , the shallow segment breaks later than the deep segment (dashed line in Figure 4c) because  $\kappa$  increases exponentially with depth for the planar fault (same as the dashed line in Figure 3c).

### 4. Discussion and Conclusions

Previous geodetic studies have found that the MHT along the entire Himalayan arc is fully locked at shallow depth with a narrowed transition zone (~20-30 km depth) to fully creeping state (Ader et al., 2012; Stevens & Avouac, 2015). This transition zone has been proposed to be temperature-dependent and bounded by 350 and 450 °C isotherms (Ader et al., 2012; Bilham et al., 2017). Under such temperatures, the fault behaves partially brittle-seismic and partially ductile-aseismic (Hyndman, 2013); hence, it represents a lower effective friction coefficient in comparison to the shallow brittle zone (Gao & Wang, 2017). Our models show that lower effective friction coefficients and/or higher dipping angles of deep segment would allow for diminished capacity to store shear stress within the seismogenic zone of a fault (Figure 2), leading to an earlier failure time as would be expected from Coulomb failure (Figures 3b and 4b). This may explain why moderate-size earthquakes (7  $< M_w < 8$ ) tend to occur more frequently in the deeper portions of the seismogenic zone of the Himalayan arc (Bilham et al., 2017) as well as subduction zones (e.g., Moreno et al., 2018). The "geometrical stress deficit" may be particularly relevant here (Figure 2a). Topography may also impact the slip processes at various depths on the fault (e.g., Elliott et al., 2016; Thompson et al., 2015), while topography is normally not considered in the earthquake slip determination with half-space models. In contrast, the shallow segment with higher effective friction strength and/or lower dipping angle has enhanced capabilities to accumulate shear stress (Figure 2), leading to a longer interseismic loading time (Figures 3c and 4c).



When the frictional-weak deep-dipping ramp segment breaks as a moderate-size earthquake, the frictional-strong shallow-dipping flat segment may be able to "absorb" static stresses transferred from deep as a "stress reservoir" until the added stresses are large enough to trigger a consequent failure of shallow segment. The "frictional stress reservoir" may be particularly relevant here (Figure 2b). In this way, shallow and deep earthquakes can therefore separately fill the long-term slip deficit accumulated through locking of the plate interface. Our results therefore provide some mechanical insights to the previously proposed strain reservoir hypothesis in Himalaya (Bilham et al., 2017; Mencin et al., 2016).

Comprehensive analysis of interseismic deformation indicates that the crustal ramp is an active structure beneath the topographic front of the Higher Himalaya (Berger et al., 2004; Grandin et al., 2012; Lindsey et al., 2018). The ramp seems spatially coincident with the clustered background microseismicity (Pandey et al., 1995), indicating that high shear stress is building up near such geometrical variation under steady tectonic loading. This observation is compatible with our modeling results that the high shear stress rate is on the ramp segment, especially on the transition area from the flat segment to the ramp segment (Figure 1b). Aftershocks also appear to concentrate on such geometrical barriers as observed following some continental earthquakes (e.g., 2015 Gorkha earthquake (Elliott et al., 2016) and 2008 Wenchuan earthquake in eastern Tibet (Qi et al., 2011)). One interesting finding of our models is that the steeper ramp would cause faster shear stress accumulated on the shallow segment and increase the seismic hazards of the entire fault. This effect is not considered in previous (analytical) geometry studies (e.g., Bletery et al., 2016). Thus, 3-D models with laterally varying dip angle of the ramp would help us to evaluate the variation of seismic potential in lateral direction (e.g., Whipple et al., 2016; Zhang et al., 2017) and may provide insights on the mechanisms of lateral seismic segmentation of large megathrust system.

Our numerical experiments are specifically designed to investigate the geometrical and frictional effects on interseismic stress accumulation and hence the coseismic failure time. Therefore, we have employed quasistatic simulations and ignored dynamic processes related to the coseismic rupture (e.g., fault overshoot or undershoot (Ide et al., 2011)) as well as the effects of earthquake cycles (e.g., earthquake supercycles (Sieh et al., 2008)). These complex phenomena need future studies with rate-state and/or slip-weakening friction laws. Previous studies either emphasize the importance of geometry or friction on the seismogenesis. Our models highlight that both factors contribute to interseismic stress accumulation and hence to failure time of large earthquakes (Figures 3 and 4). Moreover, the two factors tend to nonlinearly couple each other. For instance, the higher the friction is, the stronger the effects of dip angle on decreasing the failure time are (Figure 3). Our models further reveal the feedback of shallow and deep segments as a frictional segmented system; that is, the influence of deep segment to shallow segment (Figure 4b) is stronger than the shallow segment to the deep segment (Figure 4a) in terms of failure time. This finding supports the hypothesis that the deep segment may influence the failure of the shallow segment (Bilham et al., 2017), which is applicable to subduction zones (e.g., Konca et al., 2008; Moreno et al., 2018).

#### Acknowledgments

Shaoyang Li and William Barnhart were supported by the National Science Foundation grant EAR award 1645014. Marcos Moreno acknowledges support from the Chilean National Fund for Development of Science and Technology (FONDECYT) grant 1181479, German Science Foundation (DFG) grant MO 2310/3-1, the Millennium Nucleus The Seismic Cycle Along Subduction Zones funded by the Millennium Scientific Initiative (ICM) of the Chilean Government grant NC160025, and Research Center for Integrated Disaster Risk Management (CIGIDEN), CONICYT/FONDAP 15110017. All data presented in this paper are generated from numerical simulations by using PyLith software, which is available on the Computational Infrastructure for Geodynamics website (https://geodynamics.org/cig/software/ pylith/). We thank Roger Bilham and Matthias Rosenau for the insightful discussions. Constructive comments from Jack Loveless and an anonymous reviewer are highly appreciated. We thank the Editor Jeroen Ritsema for handling our paper. Figures in this paper are generated with the GMT software (Wessel & Smith, 1998).

#### References

- Aagaard, B. T., Knepley, M. G., & Williams, C. A. (2013). A domain decomposition approach to implementing fault slip in finite-element models of quasi-static and dynamic crustal deformation. *Journal of Geophysical Research: Solid Earth, 118*, 3059–3079. https://doi.org/10.1002/jgrb.50217
- Ader, T., Avouac, J. P., Liu-Zeng, J., Lyon-Caen, H., Bollinger, L., Galetzka, J., et al. (2012). Convergence rate across the Nepal Himalaya and interseismic coupling on the main Himalayan thrust: Implications for seismic hazard. *Journal of Geophysical Research*, 117, B04403. https://doi.org/10.1029/2011JB009071
- Allmann, B. P., & Shearer, P. M. (2009). Global variations of stress drop for moderate to large earthquakes. *Journal of Geophysical Research*, 114, B01310. https://doi.org/10.1029/2008JB005821
- Avouac, J.-P., Meng, L., Wei, S., Wang, T., & Ampuero, J.-P. (2015). Lower edge of locked main Himalayan thrust unzipped by the 2015 Gorkha earthquake. *Nature Geoscience*, 8(9), 708–711. https://doi.org/10.1038/ngeo2518
- Barnhart, W. D., Brengman, C. M., Li, S., & Peterson, K. E. (2018). Ramp-flat basement structures of the Zagros Mountains inferred from coseismic slip and afterslip of the 2017 M<sub>w</sub> 7.3 Darbandikhan, Iran/Iraq earthquake. *Earth and Planetary Science Letters*, 496, 96–107. https://doi.org/10.1016/j.epsl.2018.05.036
- Beck, S., Barrientos, S., Kausel, E., & Reyes, M. (1998). Source characteristics of historic earthquakes along the central Chile subduction askew at Alzone. *Journal of South American Earth Sciences*, 11(2), 115–129. https://doi.org/10.1016/S0895-9811(98)00005-4
- Berger, A., Jouanne, F., Hassani, R., & Mugnier, J.L. (2004). Modelling the spatial distribution of present-day deformation in Nepal: How cylindrical is the main Himalayan thrust in Nepal? *Geophysical Journal International, 156*(1), 94–114. https://doi.org/10.1111/j.1365-246X.2004.02038.x Bilham, R., & England, P. (2001). Plateau "pop-up" in the great 1897 Assam earthquake. *Nature, 410*(6830), 806–809. https://doi.org/10.1038/35071057



- Bilham, R., Mencin, D., Bendick, R., & Bürgmann, R. (2017). Implications for elastic energy storage in the Himalaya from the Gorkha 2015 earthquake and other incomplete ruptures of the main Himalayan thrust. *Quaternary International*, 462, 3–21. https://doi.org/10.1016/j. quaint.2016.09.055
- Bletery, Q., Thomas, A. M., Rempel, A. W., Karlstrom, L., Sladen, A., & De Barros, L. (2016). Mega-earthquakes rupture flat megathrusts. *Science*, 354(6315), 1027–1031. https://doi.org/10.1126/science.aag0482
- Byerlee, J. (1978). Friction of rocks. Pure and Applied Geophysics, 116(4-5), 615-626. https://doi.org/10.1007/bf00876528
- Delouis, B., Pardo, M., Legrand, D., & Monfret, T. (2009). The M<sub>w</sub> 7.7 Tocopilla earthquake of 14 November 2007 at the southern edge of the northern Chile seismic gap: Rupture in the deep part of the coupled plate interface. *Bulletin of the Seismological Society of America*, 99(1), 87–94. https://doi.org/10.1785/0120080192
- Di Toro, G., Goldsby, D. L., & Tullis, T. E. (2004). Friction falls towards zero in quartz rock as slip velocity approaches seismic rates. *Nature*, 427(6973), 436–439. https://doi.org/10.1038/nature02249
- Duan, B. (2012). Dynamic rupture of the 2011  $M_w$  9.0 Tohoku-Oki earthquake: Roles of a possible subducting seamount. *Journal of Geophysical Research*, 117, B05311. https://doi.org/10.1029/2011JB009124
- Elliott, J. R., Jolivet, R., González, P. J., Avouac, J. P., Hollingsworth, J., Searle, M. P., & Stevens, V. L. (2016). Himalayan megathrust geometry and relation to topography revealed by the Gorkha earthquake. *Nature Geoscience*, 9(2), 174–180. https://doi.org/10.1038/ngeo2623
- Feng, W., Lindsey, E., Barbot, S., Samsonov, S., Dai, K., Li, P., et al. (2017). Source characteristics of the 2015  $M_w$  7.8 Gorkha (Nepal) earthquake and its  $M_w$  7.2 aftershock from space geodesy. *Tectonophysics*, 712, 747–758.
- Galetzka, J., Melgar, D., Genrich, J. F., Geng, J., Owen, S., Lindsey, E. O., et al. (2015). Slip pulse and resonance of the Kathmandu basin during the 2015 Gorkha earthquake. Nepal. Science, 349(6252), 1091–1095. https://doi.org/10.1126/science.aac6383
- Gao, X., & Wang, K. (2014). Strength of stick-slip and creeping subduction megathrusts from heat flow observations. *Science*, 345(6200), 1038–1041. https://doi.org/10.1126/science.1255487
- Gao, X., & Wang, K. (2017). Rheological separation of the megathrust seismogenic zone and episodic tremor and slip. *Nature*, *543*(7645), 416–419. https://doi.org/10.1038/nature21389
- Gerya, T. V., Stern, R. J., Baes, M., Sobolev, S. V., & Whattam, S. A. (2015). Plate tectonics on the earth triggered by plume-induced subduction initiation. *Nature*, 527(7577), 221–225. https://doi.org/10.1038/nature15752
- Goldsby, D. L., & Tullis, T. E. (2011). Flash heating leads to low frictional strength of crustal rocks at earthquake slip rates. *Science*, 334(6053), 216–218. https://doi.org/10.1126/science.1207902
- Grandin, R., Doin, M.-P., Bollinger, L., Pinel-Puysségur, B., Ducret, G., Jolivet, R., & Sapkota, S. N. (2012). Long-term growth of the Himalaya inferred from interseismic InSAR measurement. *Geology*, 40(12), 1059–1062. https://doi.org/10.1130/G33154.1
- Hayes, G. P., Briggs, R. W., Barnhart, W. D., Yeck, W. L., McNamara, D. E., Wald, D. J., et al. (2015). Rapid characterization of the 2015 M<sub>w</sub> 7.8 Gorkha, Nepal, earthquake sequence and its seismotectonic context. Seismological Research Letters, 86(6), 1557–1567. https://doi.org/10.1785/0220150145
- Hayes, G. P., Herman, M. W., Barnhart, W. D., Furlong, K. P., Riquelme, S., Benz, H. M., et al. (2014). Continuing megathrust earthquake potential in Chile after the 2014 Iguique earthquake. *Nature*. 512(7514), 295–298. https://doi.org/10.1038/nature13677
- Hubbard, J., Almeida, R., Foster, A., Sapkota, S. N., Bürgi, P., & Tapponnier, P. (2016). Structural segmentation controlled the 2015 Mw 7.8 Gorkha earthquake rupture in Nepal. *Geology*, 44(8), 639–642. https://doi.org/10.1130/G38077.1
- Hyndman, R. D. (2013). Downdip landward limit of Cascadia great earthquake rupture. *Journal of Geophysical Research: Solid Earth, 118,* 5530–5549. https://doi.org/10.1002/jgrb.50390
- lde, S., Baltay, A., & Beroza, G. C. (2011). Shallow dynamic overshoot and energetic deep rupture in the 2011  $M_w$  9.0 Tohoku-Oki earthquake. Science, 332(6036), 1426–1429. https://doi.org/10.1126/science.1207020
- linuma, T., Ohzono, M., Ohta, Y., & Miura, S. (2011). Coseismic slip distribution of the 2011 off the Pacific coast of Tohoku earthquake (*M* 9.0) estimated based on GPS data—Was the asperity in Miyagi-oki ruptured? *Earth, Planets and Space*, 63(7), 643–648. https://doi.org/10.5047/eps.2011.06.013
- Jaeger, J. C., & Cook, N. G. W. (1979). Fundamentals of rock mechanics (p. 585). London: Chapman & Hall.
- Kanda, R. V. S., & Simons, M. (2010). An elastic plate model for interseismic deformation in subduction zones. *Journal of Geophysical Research*, 115, B03405. https://doi.org/10.1029/2009JB006611
- Kaneko, Y., Avouac, J. P., & Lapusta, N. (2010). Towards inferring earthquake patterns from geodetic observations of interseismic coupling. *Nature Geoscience*, 3(5), 363–369. https://doi.org/10.1038/ngeo843
- Konca, A. O., Avouac, J. P., Sladen, A., Meltzner, A. J., Sieh, K., Fang, P., et al. (2008). Partial rupture of a locked patch of the Sumatra megathrust during the 2007 earthquake sequence. *Nature*, 456(7222), 631–635. https://doi.org/10.1038/nature07572
- Lavé, J., & Avouac, J. P. (2000). Active folding of fluvial terraces across the Siwaliks Hills, Himalayas of central Nepal. *Journal of Geophysical Research*, 105(B3), 5735–5770. https://doi.org/10.1029/1999JB900292
- Lay, T., Kanamori, H., Ammon, C. J., Koper, K. D., Hutko, A. R., Ye, L., et al. (2012). Depth-varying rupture properties of subduction zone megathrust faults. *Journal of Geophysical Research*, 117, B04311. https://doi.org/10.1029/2011JB009133
- Lindsey, E. O., Almeida, R., Mallick, R., Hubbard, J., Bradley, K., Tsang, L. L., et al. (2018). Structural control on down-dip locking extent of the Himalayan megathrust. *Journal of Geophysical Research: Solid Earth*, 123, 5265–5278. https://doi.org/10.1029/2018JB015868
- Lindsey, E. O., Natsuaki, R., Xu, X., Shimada, M., Hashimoto, M., Melgar, D., & Sandwell, D. T. (2015). Line-of-sight displacement from ALOS-2 interferometry:  $M_w$  7.8 Gorkha earthquake and  $M_w$  7.3 aftershock. *Geophysical Research Letters*, 42, 6655–6661. https://doi.org/10.1002/2015GL065385
- Loveless, J. P., & Meade, B. J. (2011). Partitioning of localized and diffuse deformation in the Tibetan Plateau from joint inversions of geologic and geodetic observations. *Earth and Planetary Science Letters*, 303(1–2), 11–24. https://doi.org/10.1016/j.epsl.2010.12.014
- McNamara, D. E., Yeck, W., Barnhart, W. D., Schulte-Pelkum, V., Bergman, E., Adhikari, L., et al. (2017). Source modeling of the 2015  $M_w$  7.8 Nepal (Gorkha) earthquake sequence: Implications for geodynamics and earthquake hazards. *Tectonophysics*, 714-715, 21–30. https://doi.org/10.1016/j.tecto.2016.08.004
- Melgar, D., Riquelme, S., Xu, X., Baez, J. C., Geng, J., & Moreno, M. (2017). The first since 1960: A large event in the Valdivia segment of the Chilean subduction zone, the 2016 M7. 6 Melinka earthquake. Earth and Planetary Science Letters, 474, 68–75. https://doi.org/10.1016/j.epsl.2017.06.026
- Mencin, D., Bendick, R., Upreti, B. N., Adhikari, D. P., Gajurel, A. P., Bhattarai, R. R., et al. (2016). Himalayan strain reservoir inferred from limited afterslip following the Gorkha earthquake. *Nature Geoscience*, 9(7), 533–537. https://doi.org/10.1038/ngeo2734
- Michel, S., Avouac, J. P., Lapusta, N., & Jiang, J. (2017). Pulse-like partial ruptures and high-frequency radiation at creeping-locked transition during megathrust earthquakes. *Geophysical Research Letters*, 44, 8345–8351. https://doi.org/10.1002/2017GL074725



- Moreno, M., Li, S., Melnick, D., Bedford, J. R., Baez, J. C., Motagh, M., et al. (2018). Chilean megathrust earthquake recurrence linked to frictional contrast at depth. *Nature Geoscience*, 11(4), 285–290. https://doi.org/10.1038/s41561-018-0089-5
- Murphy, S., Di Toro, G., Romano, F., Scala, A., Lorito, S., Spagnuolo, E., et al. (2018). Tsunamigenic earthquake simulations using experimentally derived friction laws. *Earth and Planetary Science Letters*, 486, 155–165. https://doi.org/10.1016/j.epsl.2018.01.011
- Okada, T., Yaginuma, T., Umino, N., Kono, T., Matsuzawa, T., Kita, S., & Hasegawa, A. (2005). The 2005 M7.2 Miyagi-oki earthquake, NE Japan: Possible rerupturing of one of asperities that caused the previous M7.4 earthquake. Geophysical Research Letters, 32, L24302. https://doi.org/10.1029/2005GL024613
- Pandey, M. R., Tandukar, R. P., Avouac, J. P., Lavé, J., & Massot, J. P. (1995). Interseismic strain accumulation on the Himalayan crustal ramp (Nepal). *Geophysical Research Letters*, 22(7), 751–754. https://doi.org/10.1029/94GL02971
- Perfettini, H., Avouac, J. P., Tavera, H., Kositsky, A., Nocquet, J. M., Bondoux, F., et al. (2010). Seismic and aseismic slip on the Central Peru megathrust. *Nature*, 465(7294), 78. https://doi.org/10.1038/nature09062
- Qi, W., Xuejun, Q., Qigui, L., Freymueller, J., Shaomin, Y., Caijun, X., et al. (2011). Rupture of deep faults in the 2008 Wenchuan earthquake and uplift of the Longmen Shan. *Nature Geoscience*, 4(9), 634–640. https://doi.org/10.1038/ngeo1210
- Qiu, Q., Hill, E. M., Barbot, S., Hubbard, J., Feng, W., Lindsey, E. O., et al. (2016). The mechanism of partial rupture of a locked megathrust: The role of fault morphology. *Geology*, 44(10), 875–878. https://doi.org/10.1130/G38178.1
- Ruina, A. (1983). Slip instability and state variable friction laws. *Journal of Geophysical Research*, 88(B12), 10,359–10,370. https://doi.org/10.1029/JB088iB12p10359
- Scholz, C. H. (1998). Earthquakes and friction laws. Nature, 391(6662), 37-42. https://doi.org/10.1038/34097
- Schulte-Pelkum, V., Monsalve, G., Sheehan, A., Pandey, M. R., Sapkota, S., Bilham, R., & Wu, F. (2005). Imaging the Indian subcontinent beneath the Himalaya. *Nature*, 435(7046), 1222. https://doi.org/10.1038/nature03678
- Schurr, B., Asch, G., Rosenau, M., Wang, R., Oncken, O., Barrientos, S., et al. (2012). The 2007 M7.7 Tocopilla northern Chile earthquake sequence: Implications for along-strike and downdip rupture segmentation and megathrust frictional behavior. *Journal of Geophysical Research*, 117, B05305. https://doi.org/10.1029/2011JB009030
- Sieh, K., Natawidjaja, D. H., Meltzner, A. J., Shen, C. C., Cheng, H., Li, K. S., et al. (2008). Earthquake supercycles inferred from sea-level changes recorded in the corals of West Sumatra. Science, 322(5908), 1674–1678. https://doi.org/10.1126/science.1163589
- Simons, M., Minson, S. E., Sladen, A., Ortega, F., Jiang, J., Owen, S. E., et al. (2011). The 2011 magnitude 9.0 Tohoku-Oki earthquake: Mosaicking the megathrust from seconds to centuries. Science, 332(6036), 1421–1425. https://doi.org/10.1126/science.1206731
- Stevens, V. L., & Avouac, J. P. (2015). Interseismic coupling on the main Himalayan thrust. *Geophysical Research Letters*, 42, 5828–5837. https://doi.org/10.1002/2015GL064845
- Thompson, T. B., Plesch, A., Shaw, J. H., & Meade, B. J. (2015). Rapid slip-deficit rates at the eastern margin of the Tibetan Plateau prior to the 2008 M<sub>w</sub> 7.9 Wenchuan earthquake. *Geophysical Research Letters*, 42, 1677–1684. https://doi.org/10.1002/2014GL062833
- Wang, K., & Hu, Y. (2006). Accretionary prisms in subduction earthquake cycles: The theory of dynamic Coulomb wedge. *Journal of Geophysical Research*, 111, B06409. https://doi.org/10.1029/2005JB003987
- Wessel, P., & Smith, W. H. F. (1998). New, improved version of the generic mapping tools released. EOS Transactions AGU, 79(47), 579. https://doi.org/10.1029/98E000426
- Whipple, K. X., Shirzaei, M., Hodges, K. V., & Ramon Arrowsmith, J. (2016). Active shortening within the Himalayan orogenic wedge implied by the 2015 Gorkha earthquake. *Nature Geoscience*, *9*(9), 711–716. https://doi.org/10.1038/ngeo2797
- Yang, H., Liu, Y., & Lin, J. (2013). Geometrical effects of a subducted seamount on stopping megathrust ruptures. *Geophysical Research Letters*, 40. 2011–2016. https://doi.org/10.1002/grl.50509
- Yue, H., Simons, M., Duputel, Z., Jiang, J., Fielding, E., Liang, C., et al. (2017). Depth varying rupture properties during the 2015 M<sub>w</sub> 7.8 Gorkha (Nepal) earthquake. *Tectonophysics*, 714-715, 44–54. https://doi.org/10.1016/j.tecto.2016.07.005
- Zhang, Y., Wang, R., Walter, T. R., Feng, W., Chen, Y., & Huang, Q. (2017). Significant lateral dip changes may have limited the scale of the 2015 M<sub>w</sub> 7.8 Gorkha earthquake. *Geophysical Research Letters*, 44, 8847–8856. https://doi.org/10.1002/2017GL074095
- Zhao, W., Nelson, K. D., Che, J., Quo, J., Lu, D., Wu, C., & Liu, X. (1993). Deep seismic reflection evidence for continental underthrusting beneath southern Tibet. *Nature*, 366(6455), 557–559. https://doi.org/10.1038/366557a0